Chapter 4

All-optical Semiconductor Optical Amplifiers Using Quantum Dots (Optical Pumping)

Khalil Safari, Ali Rostami, Ghasem Rostami and Mahboubed Dolatyari

Additional information is available at the end of the chapter

http://dx.doi.org/10.5772/62107

Abstract

In the first portion of this chapter, a short review on all-optical processing is presented. Following the ideas of all-optical processing, a basic unit cell is introduced for the realization of these systems. To this end, an all-optical semiconductor optical amplifier based on quantum dots (QD-SOA) is presented and used as the basic unit cell. Then, a novel scheme for a high-speed all-optical half-adder based on quantum dot semiconductor optical amplifiers has been theoretically and extensively analyzed. We accelerate the gain recovery process in QD-SOA with a control pulse (CP) using the cross-gain modulation (XGM) effect in QD-SOA (based on a novel work reported by Rostami *et al* published in *IEEE J. Quantum Electron* in 2010). In this proposed scheme, a pair of input data streams simultaneously drives the switch to produce sum and carry. The proposed scheme is driven by the pair of input data streasms for one switch between which the Boolean XOR function is to be executed to produce a sum-bit. Then, one of the input data is utilized to drive the second switch and another is used as input data for it to produce a carry-bit. In the proposed structure, we need to use an optical attenuator to reduce the power level of the optical signal. Thee, data pulse is at least an order of magnitude stronger than the incoming pulse; thereforehowever, only the input pulse can alter QD-SOA's optical properties. Also, an all-optical cross-phase modulation (XPM) wavelength converter has been utilized to obtain an all-optical AND gate, which is logic CARRY. Logic SUM and CARRY are simultaneously realized in the proposed structure. The operation of the system is evaluated and demonstrated with a Tb/s bit rate. The proposed structure is mathematically modeled by writing rate equations and then is numerically simulated with success. High-speed operation capabilities of the proposed all-optical half-adder structure are evaluated by numerical simulation.

Keywords: All-optical Half-Adder, QD-SOA, Optical Pumping, High-speed Processing

1. Introduction

In the past few years, all-optical signal processing concepts and technologies have evolved remarkably mainly due to the discovery of semiconductor-based all-optical switches. Electronic devices such as switches and routers are not fast enough, whereas the speed of optical communication systems can reach up to 10 Tb/s [1]. Therefore, in order to realize these capabilities in optical engineering, recently, there washas been a huge motivation for researchers in this area to concentrate on the implementation of the optical digital logic gates (e.g., AND, OR, NOT, and XOR) and optical logic modules (e.g., counters, adders, subtractors, and shift registers) [2]. In SOAs, nonlinear effects such as cross-gain modulation (XGM), cross-phase modulation (XPM), four-wave mixing (FWM), and transient cross-phase modulation can all be exploited to demonstrate all-optical signal processing functions. Several schemes on all-optical processing/operations, including nonlinear materials, terahertz optical asymmetric demultiplexer (TOAD), cross gain modulation in a semiconductor optical amplifier, SOA–Mach–Zehnder interferometer (SOA–MZI), Pperiodically poled lithium niobate (PPLN) waveguide, and ultrafast nonlinear interferometer (UNI), were proposed [3]. Most of the proposed designs are based on two or more interferometric switches; a synchronization problem between different switches restricts their designs for practical implementation. QD-SOA has a remarkable ultrafast response, larger unsaturated gain, and a much faster gain recovery after gain compression than bulk SOAs, small electron relaxation times, high-saturation output power, low-noise figure, and large-gain-bandwidth product at the same time. One of basic demands for high-speed operation is high-speed carrier dynamics. In QD-SOA, there is a high-speed carrier transport, therefore high-bit-rate devices such as logic gates can be realized based on this device. It is clear that due to band offset between QDS and wetting layer (WL), capture time will be much shorter than this parameter in bulk and quantum well structures. This parameter is between femtoseconds (fs) and picoseconds (ps) in QDs and therefore this is the main reason for high-speed operation of QD-SOA-based devices and systems. The response time for gain saturation is 100 $fs^{-1}ps$, which is sufficient for a gigabit to sub-terabit optical transmission system [4]. Technology of the quantum-dot SOAs is suitable owing to its remarkably ultrafast response, which, combined with its attractive characteristics, distinguishes them from conventional SOAs. Compared to other types of amplifiers, One of other properties of the QD-SOA is a large unsaturated gain versus other type of amplifiers, which thatleadss to higher power output. Therefore, in low-injection electric pump, there is sufficient optical gain and thus less power consumption. Also, in electric pump case, optical gain can be controlled by current density and in optical pumpcase using intensity of pump signal too. QD-SOA illustrates faster gain recovery time versus other types of optical amplifiers. Thus, QD-SOA can be used for high-speed optical signal processing without distortion [5]. The all-optical logic gates, optical wavelength conversion, and in this chapter, we develop a theoretical approach for compensation of the carrier relaxation time into excited state (ES). In our model, we have considered two energy levels in both conduction and valence bands. It will be shown that applying a CP with enough energy will highly accelerate the recovery process of QD-SOA and will lead to a high-bit-rate operation of QD-SOA–MZI structure in the presence of the CP. In recent years, the optical logic based on several different schemes has

http://dx.doi.org/10.5772/62107

been demonstrated and reported, which is based on the dual-semiconductor optical amplifier Mach–Zehnder interferometer [6,7,8], semiconductor laser amplifier (SLA) loop mirror [5–8], ultrafast nonlinear interferometers [9–12], and four-wave mixing process in SOA [13] and other alternatives. In the past reported research results, there are several publications for the realization of all-optical half adders such as terahertz optical asymmetric demultiplexers and ultrafast nonlinear interferometers [14, 15]. Based on these excellent properties of QD-SOA, interferometric effect such as the Sagnac phenomenon was realized using this optical device [16–20]. Also, using nonlinear effects such as cross-phase modulation and cross-gain modulation, all-optical XOR and AND gates were implemented by Ki *et al* and finally the half-adder was implemented [16]. Considering the nonlinear properties of SOA, an all-optical half-adder operating in 10 Gbit/s was reported in Ref. [17]. Another proposal based on four-wave mixing in SOA was illustrated in Ref. [18]. The Hhalf-adder/subtractor unit based on dark–bright solitons has been reported in Ref. [19]. All-optical half-adder using planar three-core nonlinear directional coupler was presented in Ref. [20]. For completing all-optical half-adder, monolithically integrated SOA-based -MZI switches were used to provide compact size, thermal stability, high-speed compatibility, low switching energy, relative stability, and optical integration compatibility [21–23]. Here, we present a theoretical model of an ultrafast all-optical half-adder based on the two QD-SOA-based MZI, where, in the first switch, the pair of input data streams execute the Boolean XOR function to produce a sum-bit. Besides, an all-optical XPM wavelength converter has been utilized to obtain an all-optical AND gate, which is logic CARRY. Logic SUM and CARRY are simultaneously realized [24–26]. Our proposed design requires less number of switches and other auxiliaries as compared with the other half-adder circuits using semiconductor optical amplifier-based devices. The all-optical half-adder has the potential to execute the addition in the optical domain up to 2 Tb/s. The configuration of the proposed all-optical half-adders using two symmetrical QD-SOA-based MZI switches is presented as follows: Logic SUM and CARRY are simultaneously implemented to realize the all-optical half-adder. The all-optical half-adder uses only two input signals. In electrical engineering, all arithmetic-related functions including addition, subtraction, multiplication, and division are realized by two half-adders and are a prerequisite for all-optical processors [27]. Boolean functions of logic SUM and logic CARRY exactly coincide with the XOR gate and the AND gate.

2. Principles and design of proposed all-optical half-adders

The proposed structures for half-adders (schematics and SOA-based structures) are shown in Figs. 1 and 2. In order to implement the proposed half-adder in an optical domain, the all-optical XOR and AND gates are reviewed at first. To implement the all-optical XOR gate, two SOAs with cross-gain modulation are used. To implement the all-optical AND gate, binary characteristics of the XPM wavelength converter are used too. Since the operations of XOR and AND logic gates depend on XGM and XPM phenomenon in semiconductors, the maximum speed of half-adder can be increased up to the limit of XGM and XPM. The speed of operation for all-optical half-adders is limited by pulse width and recovery time in SOAs.

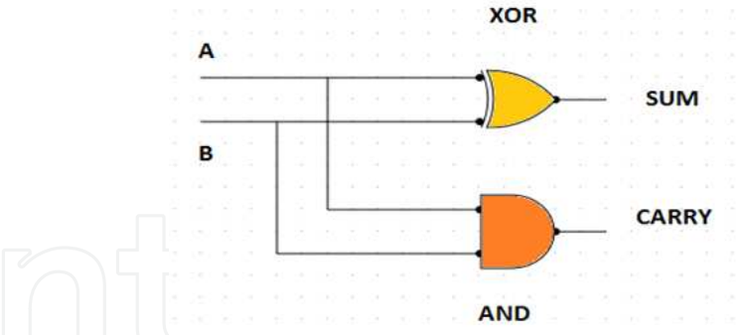

(a)

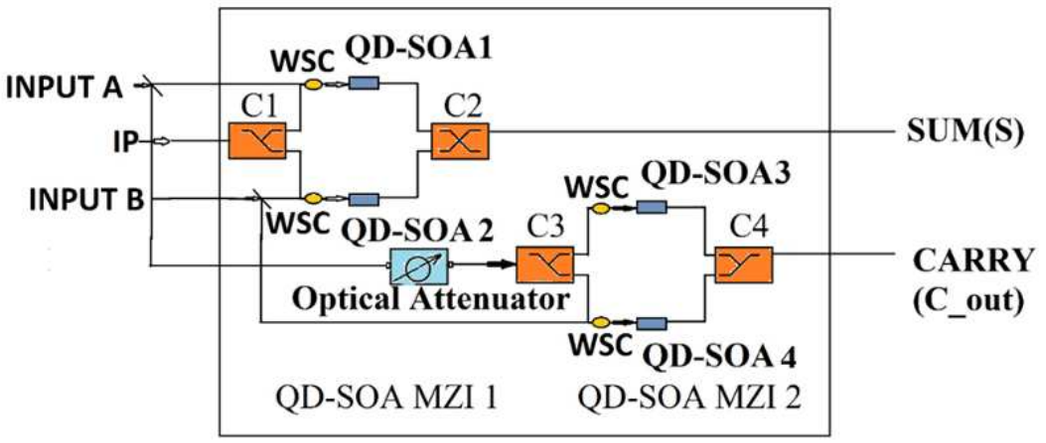

(b)

Figure 1. (a). Basic structure of half-adder [14]. (b). Half-adder without control pulse.

An electronic circuit (combinational circuits) performing addition of two binary digits is denoted as a half-adder. The carry bit will be 1 if both bits are 1, else will be zero. The sum-bit is the most significant bit of addition. A schematic of all-optical half-adders is illustrated in Fig. 2. It includes two MZIs in which QD-SOAs are in arms. For the first MZI, data inputs are A and B. Depending on data values A and B, the incoming pulse reaches Port-1 or Port-2. In this structure, output Port-1 corresponds to XOR operation and Port-2 corresponds to XNOR operation [3]. One of the attenuated input data acts as an incoming pulse for the second switch (MZI-2) and the other input data A (or B) produces the output of carry-bit. In other words, the output Port-1 of the second switch gives the logic operation AND. The four possible cases are described as follows: the input data are 1 or zero when the light beam is present or absent, respectively. Based on Fig. 2, when A=B=0, the IP signal is applied only on the first MZI. Thus, we have the signal only from Port-2 and, Port-1 will be zero and Port-2 will be 1 [3]. Therefore, Port-1 becomes inactive. It generates the output as 0, that is, carry=0. In the first switch (MZI-1), if one of the input signals (either A or B) is 0 while the other is 1, the incoming pulse emerges from the Port-1. Thuserefore, the sum (S) will be equal to 1. Now, in the second switch (MZI-2),

http://dx.doi.org/10.5772/62107

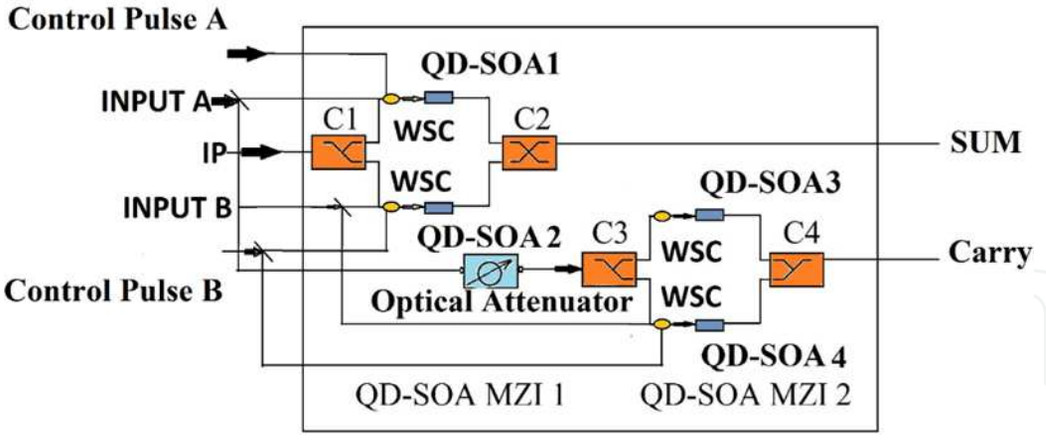

(a)

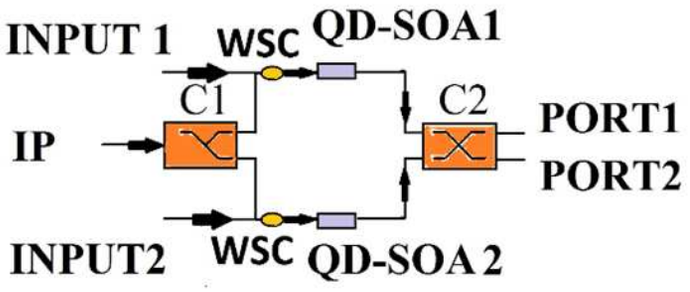

(b)

Figure 2. (a). Configuration of the proposed all-optical half-adder using two symmetrical QD-SOA-based MZI switches. (b). XOR gate [25].

AND gate produces the output as 0, that is, carry=0. When the input signal is 1 (A=B=1), the IP signal is applied on the first MZI as well. In this case, Port-2 will be 1. This way, the circuit performs the addition operation between two-bit binary data. In the next section, these theoretical results are verified through numerical simulations using Matlab [3].

3. Operational principles of QD-SOA-based MZI switch

The ease of manufacturing, installation, and operation of all-optical signal processing and communication needs integrated optics-based devices and systems [28]. As an example, the MZI is one of integrated optical building block and one can make SOA on. Thus, MZI-based SOA will be one of the integrated optical basic blocks [28]. Considering the basic principles of SOA–MZI for operation, logic gates show that it is well known when XPM and XGM or other nonlinear phenomenon in SOA is used while it is inserted in arms of MZI. In Fig. 3, a simple schematic of logic gates using SOA–MZI is shown, where SOA operates as a nonlinear element. In this structure, the pump light controls dynamics of nonlinear effects in SOA and then probe

light propagates inside the nonlinear media and experiences nonlinear optical effects. On analyzing this structure, it is observed that the control and probe fields can return to zero or non-return to zero light. Based on carrier, depletion that is occurred in SOA will conclude to gain and phase modulation which named as XGM and XPM. It should be mentioned that these effects are so efficient and thus in SOA and QD-SOA it can be realized in very short length and low pump power. As we mentioned earlier, since optical pump light is amplified in SOA, therefore low pump power is required. As shown in Fig. 3, low-gain recovery time in SOAs can be compensated in the MZI- arrangement when SOAs are in both arms as differential form. In Fig. 4, total carrier variation in SOAs using symmetric- Mach-–Zehnder (SMZ) gate-based gaiting window is illustrated. Using a control pulse with given pulse duration, a repetition rate is introduced to make a periodic variation in carrier density. When a short pulse width is used, the carrier density is depleted and also slow recovery time can be compensated by exciting both arms in MZI with suitable delay time. Based on the proposed ideas, the rise and fall times are defined by the control pulse duration [28].

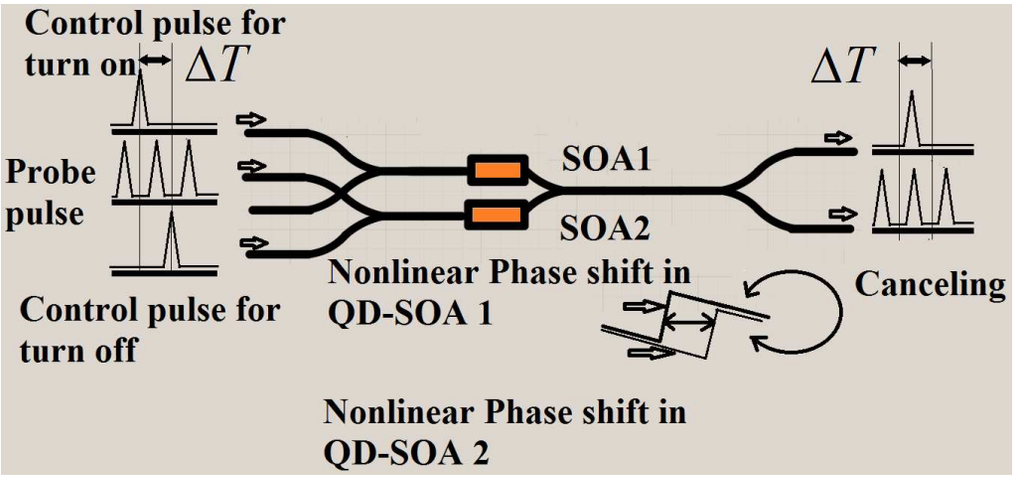

Figure 3. SMZ configuration and nonlinear phase response cancel out mechanism [26].

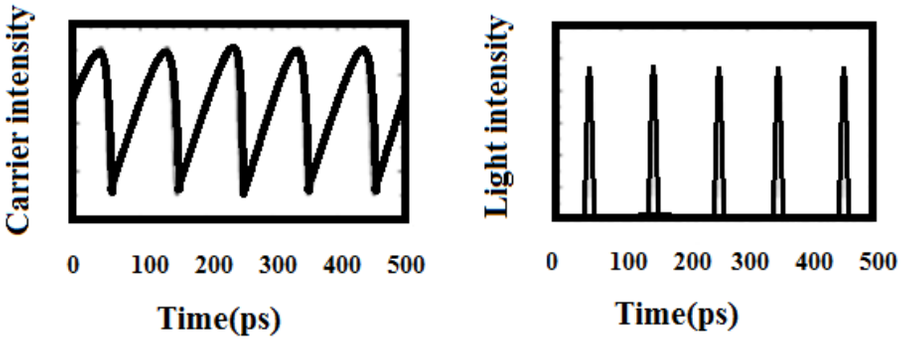

Figure 4. Total carrier density of the SOAs in the presence of control pulses (left) and SMZ gate output (right) [26].

http://dx.doi.org/10.5772/62107

3.1. SOA–MZI transfer function

MZIs with SOAs on arms are the most suitable structures for applications such as optical logic gates. Considering similar applications such as other fiber-based devices, including SOAs, and nonlinear elements, such as semiconductor laser amplifier loop optical mirror (SLALOM) and terahertz optical asymmetric demultiplexer, the SOA in MZI structure presented in Fig. 5 can be modeled with a nonlinear device with a gain effect and a phase shift applied on the input signal [28]. Therefore, the transfer function of the considered structure can be derived in the the following manner. In the above configuration, (A_1, A_2) and (D_1, D_2) are input and output lightwaves, respectively, (k_1, k_2) are normalized coupling coefficients of the input and output couplers and (B_1, B_2) and ($C1$, $C2$) are input and output lightwaves of the SOAs, respectively. The gain and phase shift of each of the SOAs are considered with (G_1, φ_1) and (G_2, φ_2) for upper and lower arms of SOAs. Thus, considering both pairs of input and output lightwaves, the following coupled equations can be obtained [28]:

$$\begin{pmatrix} B_1 \\ B_2 \end{pmatrix} = \begin{pmatrix} \cos K_1 & i\sin K_1 \\ i\sin K_1 & \cos K_1 \end{pmatrix} \begin{pmatrix} A_1 \\ A_2 \end{pmatrix} \tag{1}$$

We assumed that an optical signal travelling through the amplifier would experience an amplification of $\sqrt{G}$ gain and a phase shift of φ. Therefore,

$$\begin{pmatrix} C_1 \\ C_2 \end{pmatrix} = \begin{pmatrix} \sqrt{G_1}e^{i\Phi_1} & 0 \\ 0 & \sqrt{G_2}e^{i\Phi_2} \end{pmatrix} \begin{pmatrix} B_1 \\ B_2 \end{pmatrix} \tag{2}$$

Then, the transfer function can be described as

$$\begin{pmatrix} D_1 \\ D_2 \end{pmatrix} = \begin{pmatrix} H_{11} & H_{12} \\ H_{21} & H_{22} \end{pmatrix} \begin{pmatrix} A_1 \\ A_2 \end{pmatrix} \tag{3}$$

where

$$\begin{aligned} H_{11} &= \cos K_1 \cos K_4 \sqrt{G_1}e^{i\Phi_1} - \sin K_1 \sin K_4 \sqrt{G_2}e^{i\Phi 2} \\ H_{21} &= i(\cos K_1 \sin K_4 \sqrt{G_1}e^{i\Phi_1} + \sin K_1 \cos K_4 \sqrt{G_2}e^{i\Phi 2}) \\ H_{21} &= i(\cos K_1 \sin K_4 \sqrt{G_1}e^{i\Phi_1} + \sin K_1 \cos K_4 \sqrt{G_2}e^{i\Phi 2}) \\ H_{22} &= -\sin K_1 \sin K_4 \sqrt{G_1}e^{i\Phi_1} + \cos K_1 \cos K_4 \sqrt{G_2}e^{i\Phi 2} \end{aligned} \tag{4}$$

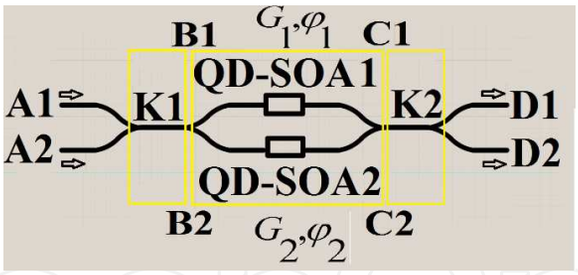

Figure 5. Schematic of SOA-incorporated MZI structure [26].

Denoting the input and output signal powers with PA1, PA2, PD1, and PD2 and assuming an ideal 3 dB coupler ($\sin k_i = \sqrt{2}/2$, $\cos k_i = \sqrt{2}/2$), the transfer function reduces to

$$H_{D1} = \frac{P_{D1}}{P_{A1}} = \frac{1}{4}G_1 + \frac{1}{4}G_2 - \frac{1}{2}\sqrt{G_1 G_2}\cos\Delta\Phi \tag{5}$$

$$H_{D2} = \frac{P_{D2}}{P_{A1}} = \frac{1}{4}G_1 + \frac{1}{4}G_2 + \frac{1}{2}\sqrt{G_1 G_2}\cos\Delta\Phi$$
$$\Delta\Phi = \Phi_1 - \Phi_2 \tag{6}$$

3.2. QD-SOA–MZI-based XOR gate

Fig. 3 depicts a schematic diagram of the all-optical QD-SOA-based MZI switch. It consists of symmetrical MZI where one QD-SOA is located in each arm of the interferometer [3,1,23]. A probe signal composed of continuous series of unit pulses at wavelength λ_p is inserted in the MZI and is split into two equal parts and travels separately along the identical QD-SOAs located in their path.

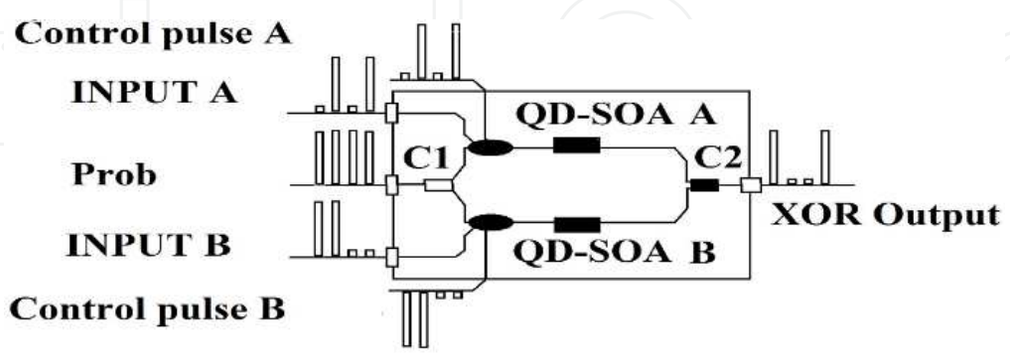

Figure 6. XOR gate based on QD-SOA [3].

The wavelength separation between λ_S and λ_p should be less than the homogeneous broadening of the single QD gain to ensure effective cross-gain modulation. The data pulse is at least

an order of magnitude stronger than the incoming pulse so that only the input pulse can alter QD-SOAs' optical properties. In the case of input data A=B=0, the traveling probe signal through the two arms of the SOA acquires a phase difference of π when it recombines at the output, and so the output is "0" due to the destructive interference. Besides, in the case of A=1, B=0, the signal traveling through the arm acquires a phase change due to the presence of XPM between the pulse train and the signal. The signal traveling through the lower arm does not have this additional phase change which results in an output "1". The same result occurs for A=0, and B=1. When A=1 and B=1, the phase changes for the signal traveling through both arms will be equal, and the output is "0". The XOR output intensity can be expressed as [27–29, 32]

$$P_{\mathrm{XOR}} = P_{\mathrm{probe}}\{k_1k_2G_A(t) + (1-k_1)(1-k_2)G_B(t) - 2\sqrt{k_1k_2(1-k_1)(1-k_2)G_A(t)G_B(t)}\} \times \cos\ [\varphi_A - \varphi_B] \quad (7)$$

Where $G_A(t)$ and $G_B\ (t)$ are defined as integrated gain of QD-SOA, $\varphi_1(t)$, $\varphi_2(t)$, are nonlinear phase shifts, k_1, k_2 are the coupling coefficients of the couplers C_1 and C_2, respectively, and, in this work, are equally set to 0.5 for simplicity. We present some recommendations for the parameter designs for practical QD-SOA devices.

1. The dynamics of gain recovery of QD-SOA is critically dependent on injection current density and electron relaxation time (τ_{w2}) from WL to QD. Injecting higher current and decreasing τ_{w2} provides faster gain recovery and consequently better gate performance. However, very high current is prohibited for practical devices.
2. Long-length QD-SOA provide high-quality factor, but high current is required to achieve the same current density.
3. Using multilayer QDs provide high density of QDs and relatively high-modal gain, but may reduce the saturation power and cause the pattern effect. Therefore, the number of QD layers should be appropriated according to the practical requirement.
4. Smaller g_0 produces narrower gate window width but lower window height.
5. Smaller α aids to produce narrower gate window. Low α value is the unique advantage of QD-SOA, so better gate performance can be expected.
6. Shorter pulse width assures smaller overlaps between pulses, and consequently high-quality output signals.
7. Relatively high-control pulse energy can improve the quality factor (Q) of the output signal [33–40].

3.3. QD-SOA–MZI-based AND gate

Logic AND operation is another important Boolean function which corresponds to the sampling of one signal with another. The AND gate is obtained using cross-phase modulation of two input signals in SOAs located in the two arms of a Mach–Zehnder interferometer built using SOAs. The principle of logic AND using the MZI involves coupling the two input signals

into ports 1 and 3 of the SOA–MZI configuration. If the operation is performed on the positive slope in the transfer function of interferometer, the input signal 2 will sample input signal 1. Therefore, the selective switching of the data pulses at λ_{AND} occurs exclusively during the mark of signal 1, which yields the logical AND operation. The structural parameters are similar to the parameters considered for XOR gate [26, 41–44].

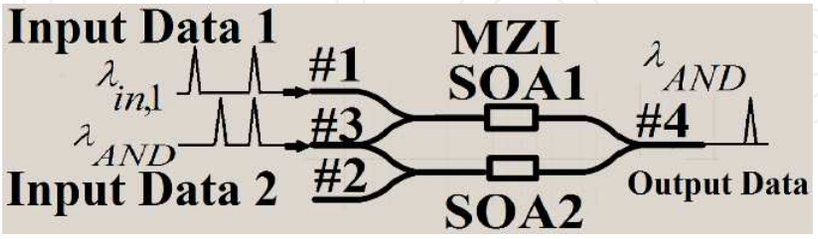

Figure 7. Configuration of a SOA–MZI structure for AND operation [26].

3.4. Metrics characterizing the quality of switching in this chapter

The quality factor $Q = 20 \times \log((P_1 - P_0)/(\sigma_1 + \sigma_0))$ where P_1, P_0, and σ_1, and σ_0 are the mean and the standard deviation of the peak power of the output's '1's and '0's, respectively. Q value is sensitive to the input pulse width and increasing the pulse width decreases the Q factor because of the overlapping of two neighboring pulses. The quality factor (Q) is dependent on Γ. Multilayer QD structures are considered as a technique to increase the modal gain due to increase in the Γ parameter and therefore reducing the current threshold. The extinction ratio (ER) is defined as $ER = 10\log\left(\frac{P^1_{MIN}}{P^0_{MAX}}\right)$ where P^1_{MIN} and P^0_{MAX} are the minimum and maximum values of the peak power of high state and low state, respectively.

4. Rate equation

The typical structure of the quantum-dot SOA is illustrated in Fig. 5. The physics of operation of SOA includes the current injection into the active layer having quantum dots, and therefore the input optical signals are amplified through the stimulated emission or the use of the optical nonlinearity by the quantum dots for this processing. Fig. 5 also shows the cross-sectional and plan-view images of self-assembled InGaAs quantum dots as a typical example of quantum-dot crystals. As it is clear, self-assembled InGaAs quantum dots on GaAs substrates and their application to semiconductor lasers have been studied since the early 1990s. They are nano-sized semiconductor islands with a wetting layer grown via the Stranski–Krastanov mode under highly mismatched epitaxy, where the electron energy states are completely quantized due to the three-dimensional quantum confinement. Quantum-dot SOAs are novel optical devices using self-assembled quantum dots [34].

http://dx.doi.org/10.5772/62107

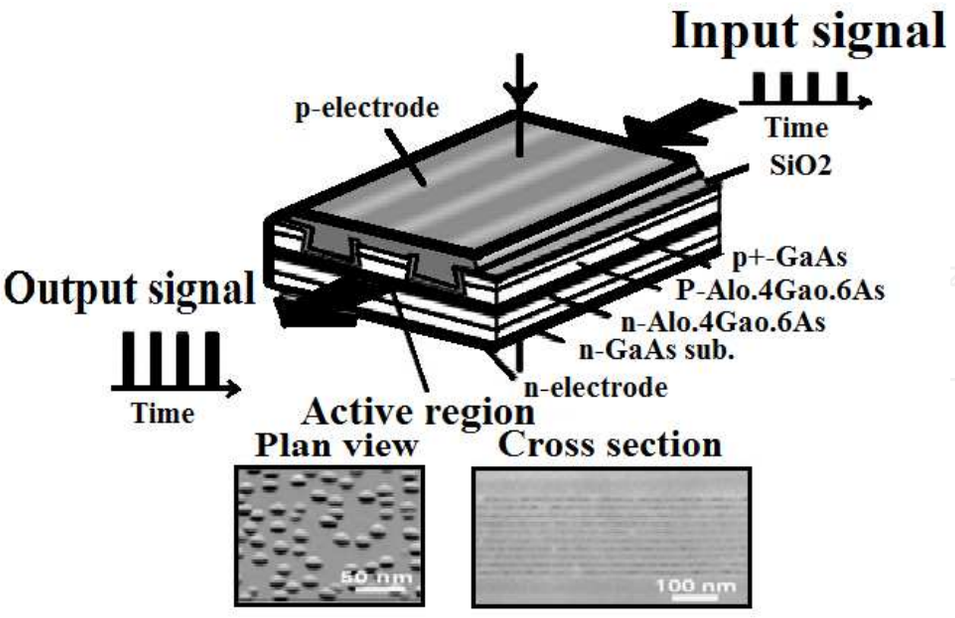

Figure 8. Structure of the quantum-dot SOA with cross-sectional and plan-view images of self-assembled InGaAs quantum dots. [34]

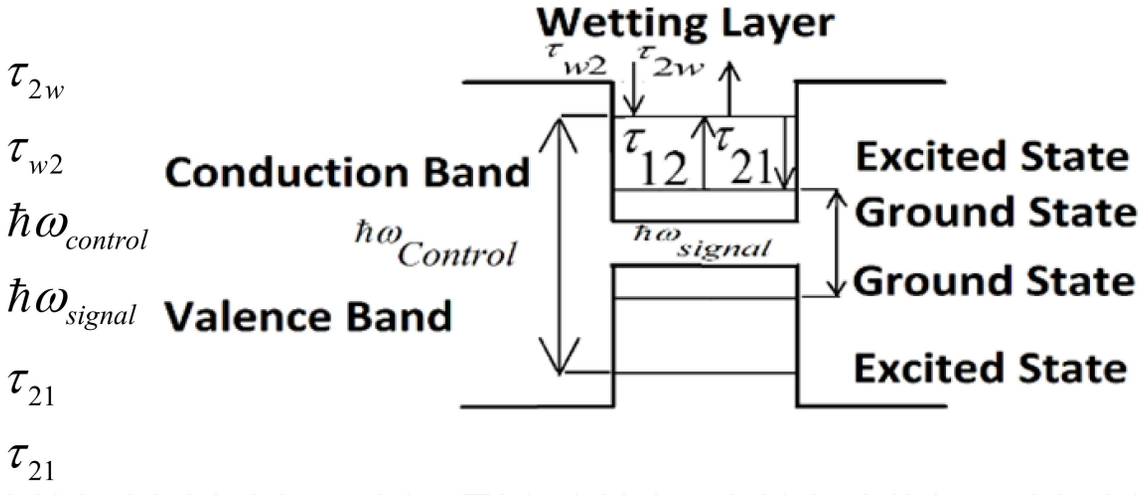

Figure 9. Band diagram of the QD structure with related energy levels [3].

In the QD-SOA–MZI, optical signals propagate in an active medium with the gain determined by the rate equations for the electron transitions in QD-SOA between WL, ground state (GS) and ES. We have considered the two energy levels in the conduction band: GS and ES. The diagram of the energy levels and electron transitions in the QD conduction band is shown in Fig. 5. The stimulated and spontaneous radiative transitions occur from GS to the QD valence band. The system of the rate equations accounts for the following transitions:

1. The fast electron transitions from WL to ES with the relaxation time 5×10^{10} cm^{-2}.

2. The fast electron transitions between ES and GS with the relaxation time from ES to GS τ_{21}=0.16 ps and the relaxation time from GS to ES τ_{21}=1.2 ps.

3. The slow transitions of electrons escaping from ES back to WL with the electron escape time τ_{2w}=1 ns.

The balance between the WL and ES is determined by the shorter time of QDs filling. Carriers relax quickly from the ES level to the GS level, while the former serves as a carrier reservoir for the latter. In general, the radiative relaxation time depends on the bias current. However, it can be shown that for moderate values of the WL carrier density N_w=(10^{14}−10^{15}), this dependence can be neglected. The spontaneous radiative time in QDs τ_{1R} remains large enough: τ_{1R}≥(0.4−0.5)ns [1]. In the case of the smaller signal detuning than the QD spectrum homogeneous broadening, the electron rate equations have the following forms [3,1,35,36]:

$$\frac{\partial S_{\text{control}}(z,\tau)}{\partial z} = (-\alpha_{\text{abs}})S_{\text{control}} \tag{8}$$

$$\frac{\partial S_{\text{signal,prob}}(z,\tau)}{\partial z} = (g(hw_{\text{signal,prob}}) - \alpha_{\text{int}})S_{\text{signal,prob}} \tag{9}$$

$$\frac{\partial N_w(z,\tau)}{\partial \tau} = \frac{J_0}{eL_w} - \frac{N_w(1-h)}{\tau_{w2}} + \frac{N_w h}{\tau_{2w}} - \frac{N_w}{\tau_{\text{wr}}} \tag{10}$$

$$\begin{aligned} \frac{\partial f(z,\tau)}{\partial \tau} &= \frac{(1-f)h}{\tau_{21}} - \frac{f(1-h)}{\tau_{12}} - \frac{f^2}{\tau_{1R}} - \frac{g_{\max,S}L}{N_Q}(2f-1) \\ &\times S_{\text{Prob}}(z,\tau)\frac{c}{\sqrt{\xi_r}} - -\frac{g_{\max,P}L}{N_Q}(2f-1)\times S_{\text{signal}}(z,\tau)\frac{c}{\sqrt{\xi_r}} \end{aligned} \tag{11}$$

$$\frac{\partial h(z,\tau)}{\partial \tau} = \frac{L_w N_w(1-h)}{N_Q \tau_{w2}} - \frac{N_w L_w h}{N_Q \tau_{2w}} - \frac{(1-f)h}{\tau_{21}} + \frac{f(1-h)}{\tau_{12}} + \frac{\alpha_{\max}L}{N_Q}(1-2h)\times S_{\text{control}}(z,\tau)\frac{c}{\sqrt{\xi_r}} \tag{12}$$

where e is the electron charge and J is the injection current density and bias current equal to 50 mA. In addition, τ_{w2} is the electron relaxation time from the WL to the ES, τ_{2w} is the electron escape time from the ES to the WL, τ_{wR} is the spontaneous radiative lifetime in WL, τ_{21} is the electron relaxation time from the ES to the GS, τ_{12} is the electron escape time from the GS to the ES, and τ_{1R} is the spontaneous radiative lifetime in the QD. N_Q is the surface density of QDs where its typical value is 5×10^{10} cm^{-2} α' N_w is the electron density in the WL, L_w is the effective thickness of the active layer, ξ_r is the SOA material permittivity and is the velocity of light in free space. The last term in eq. (5) and last two terms in eq. (6) demonstrate the

http://dx.doi.org/10.5772/62107

absorption of CP and stimulated emission in the conduction band ground state (CBGS), respectively. For simplicity, we presume an ideal facet reflectivity and neglect the amplified spontaneous emission. The time dependence of the integral QD-SOA gain and pulse-phase shift can be expressed as $G(\tau)=\exp(\int_0^L g(z', \tau)dz)$ and $\phi(\tau)=-\alpha\Big/2(\int_0^L g(z', \tau)\mathrm{d}z)$, respectively, where α is the linewidth enhancement factor (LEF). It has been discussed in several articles that linewidth enhancement factor may vary in a large interval from the experimentally measured value of 0.1 up to giant values of 60 in QDs. The set of Eqs. 8–12 with the defined initial conditions cannot be solved in a closed form but it can only be solved numerically. For this purpose, the optical pulses and the SOAs have been divided in many small segments in time and distance, respectively, and solutions have been obtained stepwise both in time and space for the temporal gain and phase changes experienced by the clock pulses in the two arms of the interferometer. These are required to calculate the characteristics of the switched-out clock pulses at the transmission and reflection port of the interferometer, expressed by the equations [25,27,28,38]

$$P_{\mathrm{XOR}} = P_{\mathrm{probe}}\{k_1k_2G_A(t)+(1-k_1)(1-k_2)G_B(t)-2\sqrt{k_1k_2(1-k_1)(1-k_2)G_A(t)G_B(t)}\}\times\cos\,[\varphi_A-\varphi_B] \tag{13}$$

$$P_{\mathrm{cross}} = P_{\mathrm{probe}}\{k_1k_2G_A(t)+(1-k_1)(1-k_2)G_B(t)+2\sqrt{k_1k_2(1-k_1)(1-k_2)G_A(t)G_B(t)}\}\times\cos\,[\varphi_A-\varphi_B] \tag{14}$$

P_{XOR}, P_{CROSS} are the transmission and reflection functions.

$$g(hw_{\mathrm{signal,prob}}) = g_{\max}(2f-1) \tag{15}$$

$$\alpha_{\mathrm{abs}} = \alpha_{\max}(1-2h)+\alpha_{\mathrm{int}}, S\,(z,\tau) = \frac{p(z,\tau)}{A_{\mathrm{eff}}V_g h\upsilon}, p(z,t) = \sum_{i=1}^{n} P_{\max}\exp\left(\frac{-4\ln 2(t-nT)^2}{\tau^2_{\mathrm{FWHM}}}\right) \tag{16}$$

The wavelengths of signal, probe, and CP are considered to be: λ_s=1.56 μm, λ_p=1.53 μm and λ_c=1.31 μm. For the following structure parameters [3,35,36, 37,39]:

$$g_{\max}=11.5\,\mathrm{cm}^{-1}, \alpha_{\mathrm{int}}=3\,\mathrm{cm}^{-1}, N_Q=5\times10^{10}\,\mathrm{cm}^{-2}, L_w=0.25\,\mu\mathrm{m},$$
$$\tau_{w2}=3\,\mathrm{ps}, \tau_{2w}=1\,\mathrm{ns}, \tau_{wR}=0.2\,\mathrm{ns}, \tau_{21}=0.16\,\mathrm{ps}, \tau_{12}=1.2\,\mathrm{ps}, \tau_{1R}=0.4\,\mathrm{ns},$$
$$W=10\ \mu\mathrm{m}, \Gamma=3\times10^{-2}, \alpha_{\max}=10\,\mathrm{cm}^{-1}, \alpha_{\mathrm{LEF}}=1, W=10\,\mu\mathrm{m}, \Gamma=3\times10^{-2}, \alpha_{\max}=10\,\mathrm{cm}^{-1}$$

5. Simulation results and discussion

Achieving high-speed signal processing, as mentioned earlier, depends strongly on WL to ES and ES to GS relaxation times. However, τ_{21} is not a limiting factor in the operation of con-

ventional QD-SOAs for 200 Gb/s. According to the reported results [1] pertaining to this case, τ_{21} is 160 fs because of longer WL to ES relaxation time. However, this parameter can be important in achieving high-speed operation in the proposed approach as a higher limit. Increasing the τ_{21}=0.4 ps relaxation time and consequence $\tau_{12}(\tau_{12}=\tau_{21}\exp[(E_2-E_1)/K_BT])$ will decrease the quality factor for XOR and AND output. K_B is the Boltzmann constant, T is the absolute temperature, and E_2-E_1 is the energy separation between the ES and GS. Numerically calculated results are illustrated in the following figures:

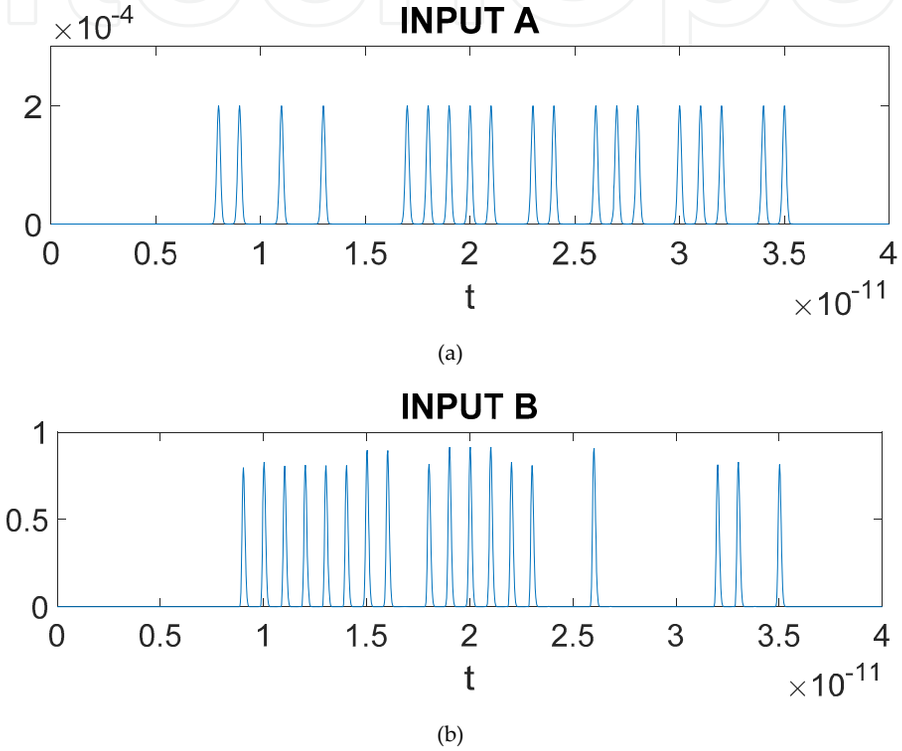

Figure 10. (a). Input waveforms of all-optical half-adder with input data stream A. (b). Input waveforms of all-optical half-adder with input data stream B.

Absorption of the CP will populate the conduction band excitation state (CBES) and hence the recovery process will accelerate, and the recovery process is much faster compared with the state where no CP is applied in the same input power and injected current.

At 2 Tb/s bit sequence, the population variation cannot reach the final population value but still varies with relatively high amplitude.

At both bit rates of 1 and 2 Tb/s, the oscillation of ES and GS completely follows the input signal variation. The simulated output waveforms are shown in Fig. 13 (a) and (b), respectively, where Fig. 13 (a) illustrates the output sum-bit and 13 (b) shows output carry-bit. Fig. 13 (c) shows that the value of ER is decreased as this relaxation time is increased to 0.4 ps. With increase in the bit-rate value from 200 Gb/s, the $ER=10\log(\frac{P^1_{MIN}}{P^0_{MAX}})$ is decreased as well.

http://dx.doi.org/10.5772/62107

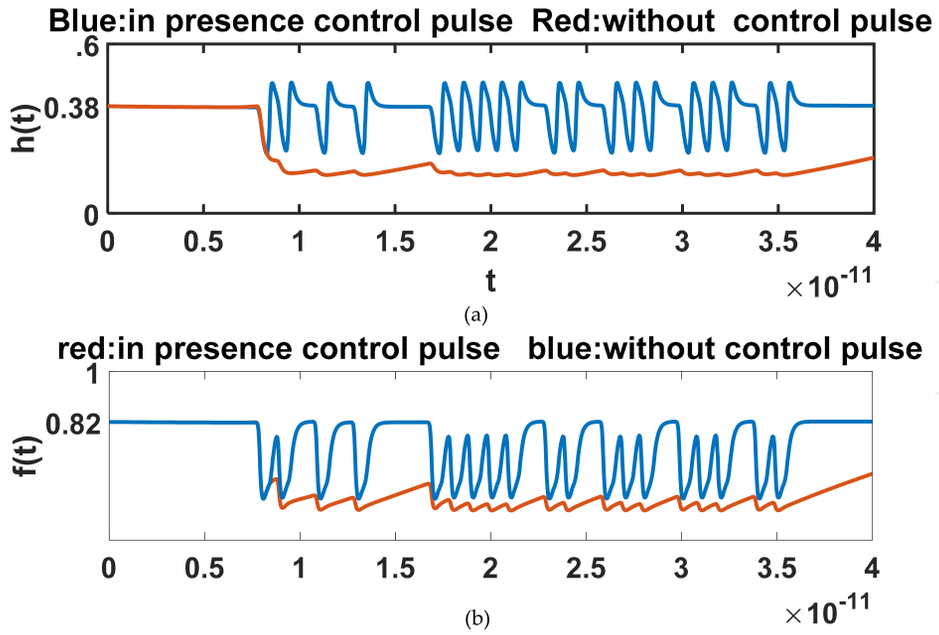

Figure 11. (a). Electron state occupation probabilities of ES, $h(t)$ with and without CP at 1 Tb/s. The bias current is 50 mA, input signal, CP, and probe signal powers are 200 UW, 250 UW, and 2 UW, respectively. (b). Electron state occupation probabilities of ES, $f(t)$ with and without CP at 1 Tb/s. The bias current is 50 mA, input signal, CP, and probe signal powers are200 UW, 250 UW, and 2 UW, respectively.

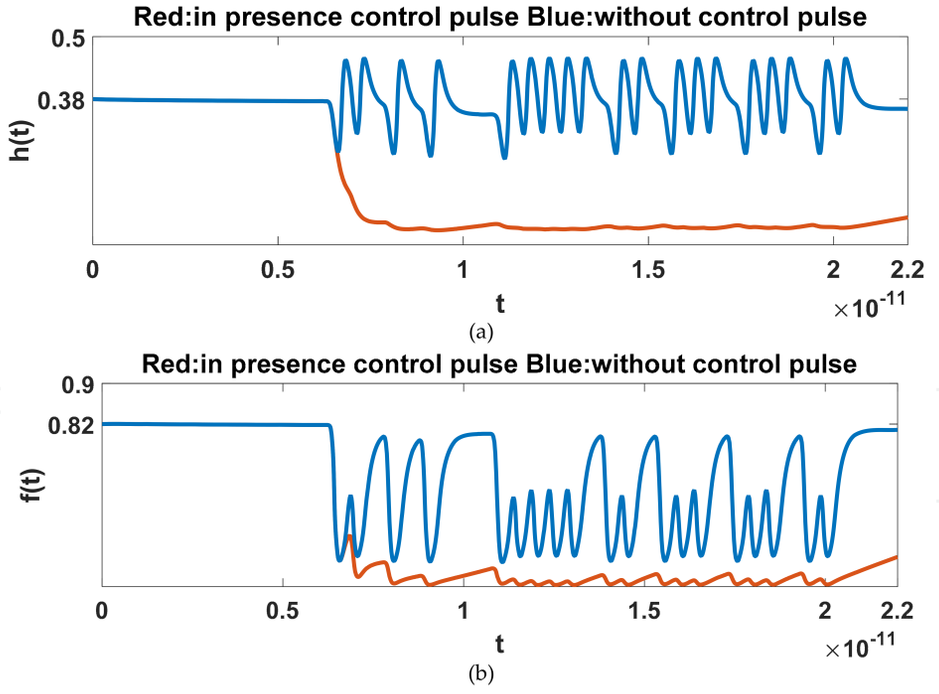

Figure 12. (a). Electron state occupation probabilities of ES, $h(t)$ with and without CP at 2 Tb/s. The bias current is 50 mA, input signal, CP, and probe signal powers are 200 UW, 250 UW, and 2 UW, respectively. (b). Electron state occupation probabilities of ES, $f(t)$ with and without CP at 2 Tb/s. The bias current is 50 mA, input signal, CP, and probe signal powers are 200 UW, 250 UW, and 2 UW, respectively.

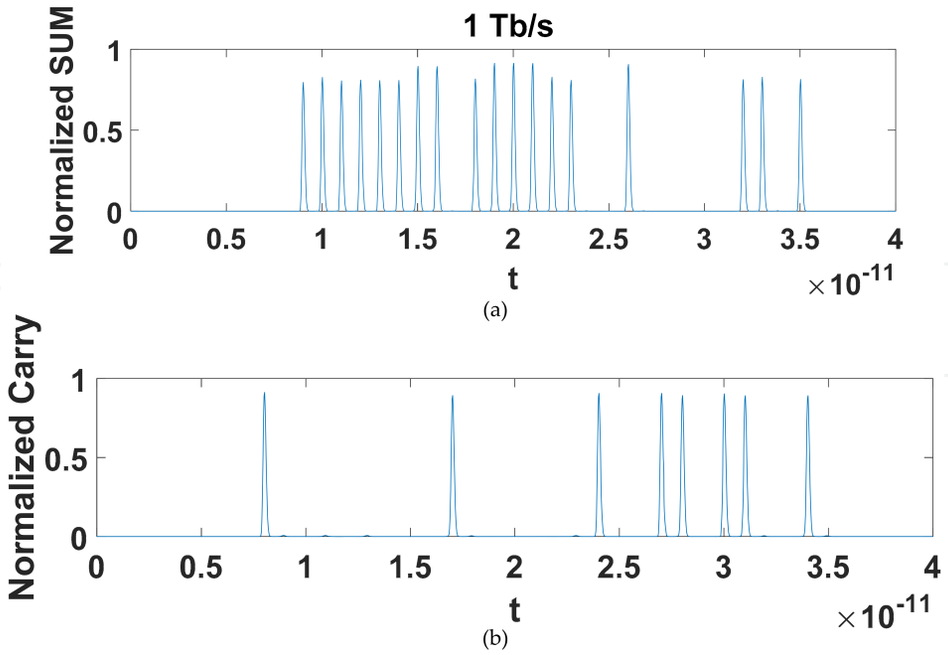

Figure 13. (a). Output waveforms of all-optical half-adders, where output sum-bit at 1Tb/s, the results describe that the pattern effect is negligible at 1 Tb/s. (b). Output waveforms of all-optical half-adders, where output carry-bit at 1 Tb/s.

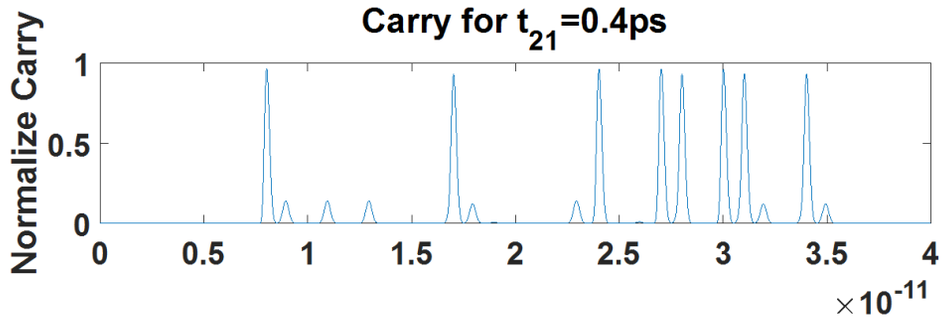

Figure 14. Output waveforms of all-optical half-adder, where output carry-bit at 1 Tb/s with $\tau_{21}=0.4ps$.

The ER is changed with the change in the electron relaxation time during electron transport from the GS to the ES. Here, the value of ER is decreased in an exponential-like manner as this relaxation time is increased. Therefore, the transition time between GS and ES must be kept low as fast as possible. The device gain is determined by the carrier density of the QD ground state. As the carrier remains longer in GS before going to the ES level,,the transition rate from the ES to GS accelerates and the ES population rapidly decreases. Decrease in the ES population reduces the gain magnitude. The WL serves as the only recipient of the pump current, while QD's excited state serves as a carrier reservoir for the GS with ultrafast carrier relaxation to the latter, and their carrier density and transition rates can affect the device gain. Therefore, the slow electron transition between ES and WL occurs, which leads to the slowing down of the cross-gain modulation process. Hence, the extinction ratio is decreased.

http://dx.doi.org/10.5772/62107

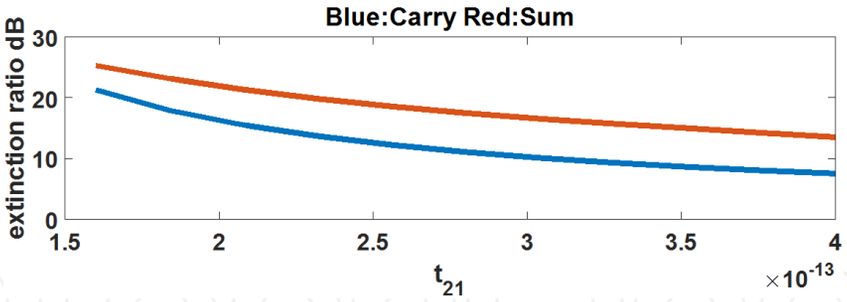

Figure 15. Variation of ER with electron relaxation time from the ES to the GS for input bit sequences at 1 Tb/s.

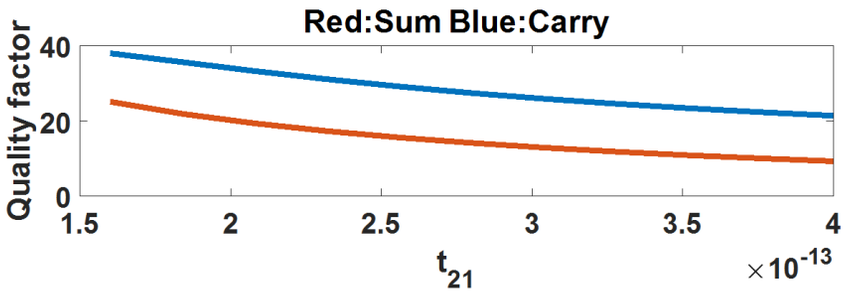

Figure 16. Quality factor with electron relaxation time from the ES to the GS for input bit sequences at 1 Tb/s.

Fig. 17 shows that the ER is very sensitive to the variations of the electron relaxation time from the ES to the GS since the slope of the curve is decreased in an exponential-like manner as this relaxation time is increased, finally becoming smoother near the left edge of the diagram. So the transition time between ES and GS must be kept below this limit and ideally be as fast as possible.

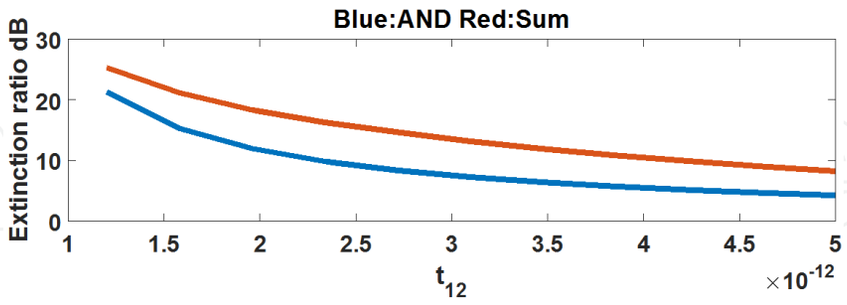

Figure 17. Variation of ER with electron relaxation time from the GS to the ES for input bit sequences at 1 Tb/s.

Fig. 18 illustrates the effect of sum with peak power of the input data signals on the ER. The characteristic of the curve is that the ER increases with power.

Fig. 19 illustrates the effect of carry with peak power of the input data signals on the ER. The characteristic of the curve is that the ER is increased with power up to a certain value after that it is decreased.

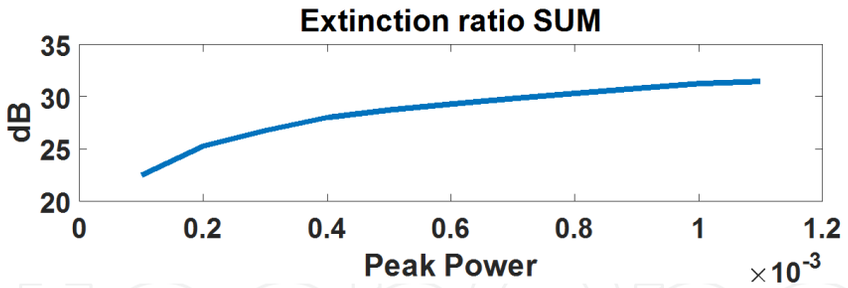

Figure 18. Variation of extinction ratio (ER) with peak data power for sum-bit, keeping other parameters fixed.

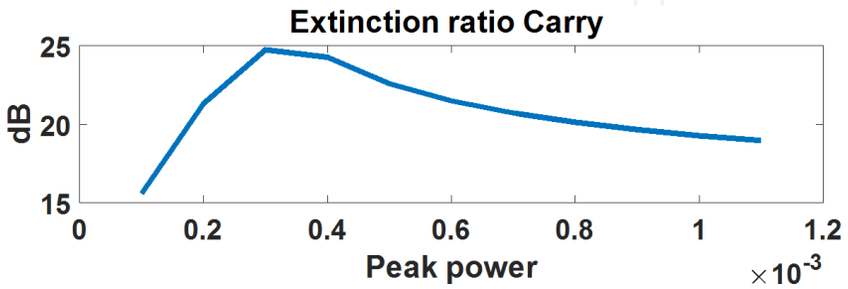

Figure 19. Variation of extinction ratio (ER) with peak data power for carry bit, keeping other parameters fixed.

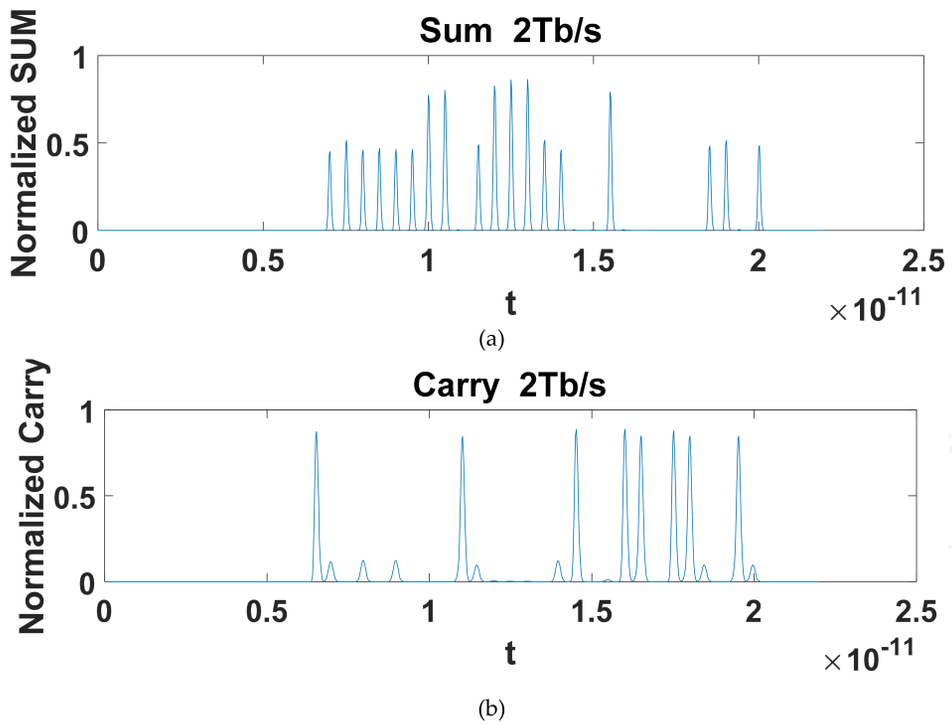

Figure 20. (a). Output waveforms of all-optical half-adder, sum-bit at 2 Tb/s. (b). Output waveforms of all-optical half-adder, carry-bit at 2 Tb/s.

The quality factor and ER are decreased with bit rate since at 2 Tb/s bit sequence, the population variation cannot reach the final population value but still varies with relatively high amplitude.

http://dx.doi.org/10.5772/62107

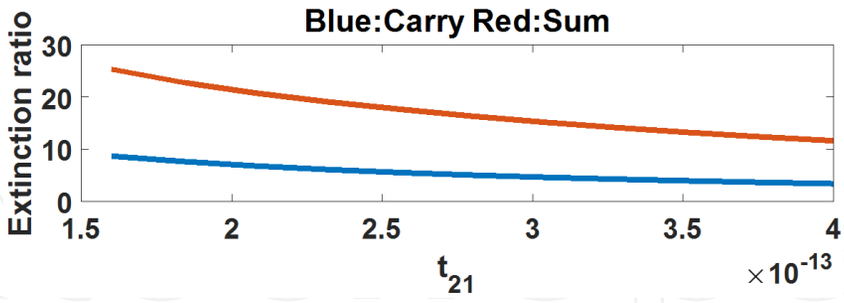

Figure 21. Variation of ER with electron relaxation time from the ES to the GS for input bit sequences at 2 Tb/s.

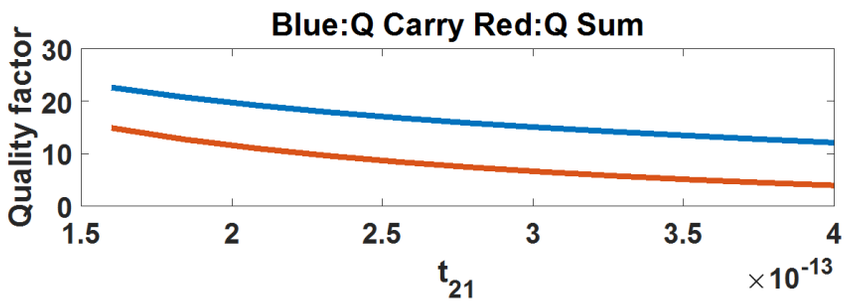

Figure 22. Quality factor with electron relaxation time from the ES to the GS for input bit sequences at 2 Tb/s.

6. Conclusion

A novel model of ultrafast all-optical half-adder using two QD-SOAs-based Mach–Zehnder interferometer was theoretically investigated and demonstrated. Numerically simulated results confirming the described method are also given in this chapter. The variation of ES to GS relaxation time on the ER and *Q*-factor at the output has been thoroughly investigated. We enhanced the bit rate, *Q* factor, and extinction ratio parameters for the half-adder. We introduced theoretical approaches to compensate the slow-carrier transition relaxation time from WL to ES (using XGM effect) which is the main limit to achieve higher speeds in QD-SOAs. It is concluded that the proposed approach accelerates the recovery process of the SOA. Applying a CP to the two-energy level QD at certain times enables the QD-SOA–MZI-based half-adder to operate under 1 and 2 Tb/s input bit sequences. This capability of control-pulse-assisted QD-SOA is promising for ultrahigh-speed all-optical logic gates, all-optical switching, and processing. The model can be extended for studying more complex all-optical circuits of enhanced functionality in which this proposed circuit developed in this paper may be assumed as the basic building block.

Author details

Khalil Safari[1], Ali Rostami[1,2*], Ghasem Rostami[2] and Mahboubed Dolatyari[2]

*Address all correspondence to: rostami@tabrizu.ac.ir

1 Photonics and Nanocrystal Research Lab. (PNRL), Faculty of Electrical and Computer Engineering, University of Tabriz, Tabriz, Iran

2 SP-EPT Labs., ASEPE Company, Industrial Park of Advanced Technologies, Tabriz, Iran

References

[1] Y. Ben-Ezra, B. I. Lembrikov, and M. Haridim, "Ultrafast all-optical processor based on quantum-dot semiconductor optical amplifiers," *IEEE J. Quantum Electron.*, vol. 45, no. 1, pp. 34–41, 2009.

[2] B. Dai, S. Shimizu, X. Wang, and N. Wada, "Simultaneous all-Optical half-adder and half-subtracter based on two semiconductor optical amplifiers," *IEEE Photonics Technol*. Lett., 2012.

[3] D. K. Gayen, D. Kumar, and T. Chattopadhyay, "Designing of optimized all-optical half adder circuit using single quantum-dot semiconductor optical amplifier assisted Mach-Zehnder interferometer," *J. Lightwave Technol.,* vol. 31, no. 12, pp. 2029–2035, 2013.

[4] A. Rostami, H. B. A. Nejad, R. M. Qartavol, and H. R. Saghai, "Tb/s optical logic gates based on quantum-dot semiconductor optical amplifiers," *IEEE J. Quantum Electron.*, vol. 46, no. 3, pp. 354–360, 2010.

[5] L. M. Sa, H. Silva, P. Andre, and R. Nogueira, "Simulation performance of all-optical logic gate XOR at 40 Gbit/s using quantum-dot SOAs," *2011 IEEE EUROCON – International Conference on Computer as a Tool*, 2011.

[6] H. L. Minh, F. Z. Ghassemlooy, and W. P. Ng, "All-optical flip-flop based on a symmetric Mach-Zehnder switch with a feedback loop and multiple forward set/reset signals," *Opt. Eng*., vol. 46, no. 4, pp. 40501–40503, 2007

[7] H. Sun, Q. Wang, H. Dong, and N. K. Dutta, "XOR performance of a quantum dot semiconductor optical amplifier based Mach-Zehnder interferometer," *Opt. Exp.*, vol. 13, no. 6, pp. 1892–1899, 2005.

[8] R. Clavero, F. Ramos, J. M. Martinez, and J. Marti, "All-optical flip-flop based on a single SOA-MZI," *IEEE Photonics Technol. Lett.*, vol. 17, no. 4, pp. 843–845, 2005.

[9] S. Diez, E. Hilliger, M. Kroh, C. Schmidt, C. Schubert, H. G. Weber, L. Occhi, L. Schares, G. Guekos, and L. K. Oxenloewe, "Optimization of SOA based Sagnac inter-

ferometer switches for demultiplexing to 10 and 40 Gbit/s," *Opt. Commun.,* vol. 189, no. 4–6, pp. 241–249, 2001.

[10] W. Hong, D. Huang, and G. Zhu, "Switching window of an SOA loop mirror with SOA sped-up by a CW assist light at transparency wavelength," *Opt. Commun.,* vol. 238, no. 1–3, pp. 151–156, 2004.

[11] K. E. Zoiros, J. Vardakas, T. Houbavlis, and M. Moyssidis, "Investigation of SOA-assisted Sagnac recirculating shift register switching characteristics," *Int. J. Light Electron Opt.*, vol. 116, no. 11, pp. 527–541, 2005.

[12] J. N. Roy and D. K. Gayen, "Integrated all-optical logic and arithmetic operations with the help of TOAD based interferometer device-alternative approach," *Appl. Opt*., vol. 46, no. 22, pp. 5304–5310, 2007.

[13] S. J. Savage, B. S. Robinson, S. A. Hamilton, and E. P. Ippen, "All-optical pulse regeneration in an ultrafast nonlinear interferometer with faraday mirror polarization stabilization," *Opt. Lett*., vol. 28, no. 1, pp.13–15, 2003.

[14] D. Gayen, A. Bhattacharyya, and J. Roy, "Ultrafast all-optical half adder using quantum-dot semiconductor optical amplifier-based Mach-Zehnder interferometer," J. Lightwave Technol., 2012.

[15] D. Li, X. Zhang, and D. Huang, "Novel all-optical format conversion using an ultrafast nonlinear interferometer at 10-40 Gbit/s," *Microw. Opt. Technol. Lett*., vol. 49, no. 3, pp. 508–510, 2007.

[16] K. E. Zoiros, P. Avramidis, and C. S. Koukourlis, "Performance investigation of semiconductor optical amplifier based ultrafast nonlinear interferometer in nontrivial switching mode," *Opt. Eng*., vol. 47, no.11, pp. 115006–115011, 2008.

[17] T. Siarkos and K. E. Zoiros, "Performance of single semiconductor optical amplifier based ultrafast nonlinear interferometer with clock control signals timing deviation in dual rail switching mode," *Opt. Eng.*, vol. 48, no. 8, pp. 85004–85012, 2009.

[18] L. Han, H. Wen, H. Zhang, and Y. Guo, "All-optical wavelength conversion for polarization shift keying signal based on four-wave mixing in a semiconductor optical amplifier," *Opt. Eng*., vol. 46, no. 9, pp. 090501–090503, 2007.

[19] J. H. Kim, Y. T. Byun, Y. M. Jhon, S. Lee, D. H. Woo, and Sun Ho Kim. "All-optical half adder using semiconductor optical amplifier based devices,"*Optics Commun.*, vol. 218, no. 4, pp. 345-349, 2003

[20] [20]Z. Chen, "Simple novel all-optical half adder," Opt. Eng., vol. 49, no.4, pp. 043201–043206, 2010

[21] [21]J. H. Kim, Y. T. Byun, Y. M. Jhon, S. Lee, D. H. Woo, and S. H. Kim, "All-optical half adder using semiconductor optical amplifier based devices," *Opt. Commun*., vol. 218, no. 4–6, pp. 345–349, 2003.

[22] S. H. Kim, J. H. Kim, J. W. Choi, C.W. Son, Y. T. Byun, Y. M. Jhon, S. Lee, D. H. Woo, and S. H. Kim, "All-optical half adder using cross-gain modulation in semiconductor optical amplifiers," *Opt. Exp.,* vol. 14, no. 22, pp. 10693–10698, 2006.

[23] P. L. Li, D. X. Huang, X. L. Zhang, and G. X. Zhu, "Ultrahigh speed all-optical half adder based on four-wave mixing in semiconductor optical amplifier," *Opt. Exp.*, vol. 14, no. 24, pp. 11839–11847, 2006.

[24] P. Phongsanam, S. Mitatha, C. Teeka, and P. P. Yupapin, "All optical half adder/subtractor using dark-bright soliton conversion control," *Microw. Opt. Technol. Lett*., vol. 53, no. 7, pp. 1541–1544, 2011.

[25] J. W. M. Menezes, W. B. Fraga, A. C. Ferreira, G. F. Guimaraes, A. F. G. F. Filho, C. S. Sobrinho, and A. S. B. Sombra, "All-optical half adder using all-optical XOR and AND gates for optical generation of "Sum" and "Carry"," *Fiber Integr. Opt.*, vol. 29, no. 4, pp. 254–271, 2010.

[26] R. P. Schreieck, M. H. Kwakernaak, H. Jackel, and H. Melchior, "All-optical switching at multi-100-Gbit/s data rates with Mach-Zehnder interferometer switches," *IEEE J. Quantum Electron*., vol. 38, no. 8, pp. 1053–1061, 2002.

[27] A. Kumar, S. Kumar, and S. K. Raghuwanshi, "Implementation of full-adder and full-subtractor based on electro-optic effect in Mach–Zehnder interferometers," *Opt. Commun*., 2014.

[28] A. Rostami, "Applications and Functionalities, "*Eng. Mater*, 2011.

[29] S. Nakamura, Y. Ueno, K. Tajima, J. Sasaki, T. Sugimoto, T. Kato, T. Shimoda, M. Itoh, H. Hatakeyama, T. Tamanuki, and T. Sasaki, "Demultiplexing of 168-Gb/s data pulses width a hybrid-integrated symmetric Mach-Zehnder all-optical switch," *IEEE Photon. Technol. Lett.*, vol. 12, no. 5, pp. 425–427, 2000.

[30] D. K. Gayen, A. Bhattachryya, T. Chattopadhyay, and J. N. Roy, "Ultrafast all-optical half adder using quantum-dot semiconductor optical amplifier based Mach-Zehnder interferometer," *J. Lightwave Technol*., vol. 30, no. 21, pp. 3387-3393, 2012.

[31] [31]A. Rostami, H. Baghban, R. Maram, "Nanostructure Semiconductor Optical Amplifiers," Berlin, Germany: Springer-Verlag, 2011.

[32] J. Y. Kim, J. M. Kang, T. Y. Kim, and S. K. Han, "All-optical multiple logic gates with XOR, NOR, OR, and NAND functions using parallel SOA-MZI structures: Theory and experiment," *J. Lightwave Technol*., vol. 24, no. 9, pp. 3392–3399, 2006.

[33] H. Sun, Q. Wang, H. Dong, and N. K. Dutta, "XOR performance of a quantum-dot semiconductor optical amplifier based Mach-Zender interferometer," *Opt. Exp.*, vol. 13, no. 6, pp. 1892–1899, 2005.

[34] E. Dimitriadou and K. E. Zoiros, "On the feasibility of ultrafast all-optical NAND gate using single quantum-dot semiconductor optical amplifier-based Mach-Zehnder interferometer," *Opt. Laser Technol.*, vol. 44, no. 6, pp. 1971–1981, 2012.

[35] E. Dimitriadou and K. E. Zoiros, "Proposal for all-optical NOR gate using single quantum-dot semiconductor optical amplifier-based Mach-Zehnder interferometer," *Opt. Commun.,* vol. 285, pp.1710–1716, 2012.

[36] E. Dimitriadou and K. E. Zoiros, "On the design of ultrafast all-optical NOT gate using quantum-dot semiconductor optical amplifier based Mach-Zehnder interferometer," *Opt. Laser Technol*., vol. 44, pp.600–607, 2012.

[37] J. Wang, Y. Jiao, R. Bonk, W. Freude, and J. Leuthold, "Regenerative properties of bulk and quantum-dot SOA based all-optical Mach-Zehnder interferometer DPSK wavelength converters," in *Proc. Conf. Photon. Switching*, October 16–18, 2006, pp. 1–3.

[38] H. Han, M. Zhang, P. Ye, and F. Zhang, "Parameter design and performance analysis of an ultrafast all-optical XOR gate based on quantum-dot semiconductor optical amplifiers in nonlinear Mach-Zehnder interferometer," *Opt. Commun.,* vol. 281, no. 20, pp. 5140–5145, 2008.

[39] M. Sugawara, H Ebe, N. Hatori, M. Ishida, Y. Arakawa, T. Akiyama, K. Otsubo, and Y. Nakata,"Theory of optical signal amplification and processing by quantum-dot semiconductor optical amplifiers," Phys. Rev., B 69, 235332-1-39 (2004)

[40] O. Qasaimeh, "Characteristics of cross-gain (XG) wavelength conversion in quantum dot semiconductor optical amplifier," *IEEE Photon.Technol. Lett.*, vol. 16, no. 2, pp. 542–544, 2004.

[41] T. W. Berg, S. Bischoff, I. Magnusdottir, and J. Mark, "Ultrafast gain recovery and modulation limitations in self-assembled quantum-dot devices," *IEEE Photon. Technol. Lett.*, ser. 6, vol. 13, pp. 541–543, 2001.

[42] T. W. Berg and J. Mark, "Saturation and noise properties of quantum-dot optical amplifiers," *IEEE J. Quantum Electron*., vol. 40, no. 11, pp. 1527–1539, 2004.

[43] J. Wang, Y. Jiao, R. Bonk, W. Freude, and J. Leuthold, "Regenerative properties of bulk and quantum-dot SOA based all-optical Mach-Zehnder interferometer DPSK wavelength converters," in Proc. Conf. Photon. Switching, October 16–18, 2006, pp. 1–3.

[44] C. I. Sandall, C. L. Walker, P. M. Smowton, D. J. Mowbray, H. Y. Liu, and M. Hopkinson, "Measurement of modal absorption, gain and recombination in p-doped and intrinsic quantum dot structures," Proc. IEE Optoelectron., vol. 153, no. 6, pp. 316–320, 2006.

IntechOpen